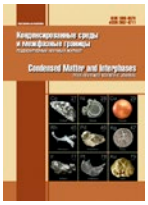

ISSN 1606-867X (Print)
ISSN 2687-0711 (Online)
Condensed Matter and Interphases
Kondensirovannye Sredy i Mezhfaznye Granitsy
https://journals.vsu.ru/kcmf/

Original articles

Research article
https://doi.org/10.17308/kcmf.2024.26/11813

Simple synthesis of floating Fe_2O_3/Luffa catalysts for the photo-Fenton degradation of methyl orange at near neutral pH

Quynh Nhu Le Thi[1, 2], Thi Quynh Trang Ly[1, 2], Anh Tien Nguyen[3], Quoc Thiet Nguyen[4], De-Hao Tsai[5], and Tien Khoa Le[1,2]✉

[1]Faculty of Chemistry, University of Science, Ho Chi Minh city, Vietnam

[2]Faculty of Chemistry, University of Science, Vietnam National University, Ho Chi Minh City, Vietnam

[3]Ho Chi Minh City University of Education, Ho Chi Minh City, Vietnam

[4]Institute of Applied Materials Science, Vietnam Academy of Science and Technology, 1B TL29 District 12, Ho Chi Minh City, Vietnam

[5]Department of Chemical Engineering, National Tsing Hua University, Hsinchu, Taiwan, ROC

Abstract

Although widely used in the textile industry, methyl orange is considered one of the most toxic dyes, which have negative impacts on the aquatic environment and needs to be removed from water bodies. Hence, the present paper reports the synthesis of new floating photo-Fenton catalysts based on the immobilization of Fe_2O_3 nanoparticles on the surface of Luffa sponges for the oxalate-induced-degradation of methyl orange. The floating catalytic sponges were prepared through a simple precipitation method followed by a reflux heating process and then characterized by field emission scanning electron microscopy, X-ray diffraction, atomic absorption spectrometry, and nitrogen adsorption-desorption experiments. According to the experimental results, methyl orange was effectively degraded over our floating catalytic sponges under light illumination at near neutral pH. The catalytic activity was also found to be enhanced with the increase in crystallinity of Fe_2O_3 nanoparticles, which can be achieved by the reflux heating. Besides, owing to the floating feature, these sponges are easily separated from the solution, thereby not forming a secondary source of pollution for water.

Keywords: Photo-Fenton catalyst; Floating material; Fe_2O_3; Luffa; Crystallinity

Funding: The research is funded by University of Science, VNU-HCM under grant number U2022-11.

For citation: Le T. Q. N., Ly T. Q. T., Nguyen A. T., Nguyen Q. Th., Tsai D.-H., Le T. Kh. Simple synthesis of floating Fe_2O_3/Luffa catalysts for the photo-Fenton degradation of methyl orange at near neutral pH. *Condensed Matter and Interphases*. 2024;26(1): 68–77. https://doi.org/10.17308/kcmf.2024.26/11813

Для цитирования: Ле Т. К. Н., Ли Т. К. Ч., Нгуен А. Т., Нгуен К. Т., Цай Д.-Х., Ле Т. К. Простой синтез плавающих фотокатализаторов Fe_2O_3/Luffa по типу Фентона для деградации метилоранжа при значении pH, близком к нейтральному. *Конденсированные среды и межфазные границы*. 2024;26(1): 68–77. https://doi.org/10.17308/kcmf.2024.26/11813

✉ Tien Khoa Le, e-mail: ltkhoa@hcmus.edu.vn

1. Introduction

Due to the dyeing efficiency without mordant and the affordable prices of azo dyes, they have been extensively used and become the most important class of synthetic dyes in the textile industry [1]. Among different azo dyes, methyl orange is an anionic, water-soluble sulfonated azo dye which is able to give the vibrant orange color to numerous materials, such as cotton, paper, nylon, and leather [2]. Nevertheless, like other azo dyes, methyl orange was reported to be toxic, potentially carcinogenic, and thereby harmful to the natural environment [3, 4]. In addition, since methyl orange contains azo groups (-N=N-) as well as aromatic groups, this organic dye is highly resistant and hardly remediated by conventional physical or biological methods [5]. Hence, the removal of methyl orange from effluents should require the advanced oxidation process using photocatalysts [6] or photo-Fenton catalysts [7] in order to degrade methyl orange molecules to smaller fractions which can be possibly eliminated by further biological treatments [2]. In fact, this azo dye was reported to be decomposed under visible light by a heterogeneous catalytic system based on Fe_2O_3/TiO_2 nanoparticles which follow both photocatalytic and photo-Fenton mechanisms [8]. Likewise, α-Fe_2O_3 with different morphologies (croissant-like structures, urchin-like structures, and textured microspheres) were successfully prepared via hydrothermal method and applied as photo-Fenton catalyst for the degradation of methyl orange under UV-C light in the presence of H_2O_2 [9]. However, most of these catalysts were used in the form of fine powders, when dispersed in effluents, they are difficult to be separated from the water body and easily become a source of secondary pollution.

In view of practical applications, the immobilization of catalytic Fe_2O_3 on a recoverable substrate could be of great benefit. It was reported that Fe_2O_3 particles can be deposited on various fiber substrates such as cellulose [10], fiberglass [11], carbon fiber cloth [12], etc. Recently, Luffa sponges, derived from the fruit of Luffa cylindrica, have attracted much attention in serving as a low-cost and eco-friendly substrate/support for inorganic catalysts [13, 14]. This natural net-like material provides fibrous strand morphologies with high porosity and high adsorption capacity [15]. Moreover, Luffa sponges have low density, which allow them to float on the water surface. Hence, the combination between photo-Fenton catalysts and Luffa sponges is expected to facilitate the light absorption of catalysts as well as the separation of catalysts from the effluents after the treatment.

However, to the best of our knowledge, the application of α-Fe_2O_3 nanoparticles deposited on Luffa sponges as floating photo-Fenton catalysts for the degradation of methyl orange still remains unexplored. Furthermore, the synthesis of α-Fe_2O_3/Luffa sponges is also a challenge. Generally, the immobilization of α-Fe_2O_3 on a substrate could be started by the precipitation of Fe^{3+} ions in the form of $Fe(OH)_3$ on the substrate surface, followed by the annealing at high temperatures to transform $Fe(OH)_3$ to α-Fe_2O_3. But this annealing step can destroy the floating α-Fe_2O_3/Luffa catalyst since the Luffa fibers are not able to withstand temperatures above 200 °C. Therefore, in this work, we proposed to synthesize new floating α-Fe_2O_3/Luffa sponge catalysts by a reflux heating process at about 100 °C instead of annealing at high temperatures. These recoverable photo-Fenton catalysts were used to degrade methyl orange under both UVA light and visible light in the presence of oxalic acid as a radical-producing source.

2. Experimental

2.1. Materials and reagents

In this work, $H_2C_2O_4 \cdot 2H_2O$ (> 98%), NaOH (⩾ 97%) and methyl orange (indicator grade) were purchased from Xilong Scientific Co., Ltd. (China). $Fe(NO_3)_3 \cdot 9H_2O$ (⩾ 98.5%) was obtained from Shanghai Zhanyun Chemical Co., Ltd (China). All these chemical reagents were used as received, without purification. The dried Luffa fruits were purchased from VINHANDS Co. (Ho Chi Minh city, Vietnam) and subsequently cut into rectangular sponges with dimensions of 20×30 mm and thickness of 5 mm. They were washed with deionized water several times and treated with NaOH solution (0.1 mol·L^{-1}) at 80 °C for 2 hours in order to remove lignin, natural oils, waxes and other impurities. This step is also necessary to support the interactions between catalyst particles and Luffa fibers. Then, the sponges were rinsed with deionized water to remove the

left over NaOH from their surface, dried at 100 °C to obtain the pretreated Luffa sponges for the immobilization of Fe_2O_3 nanoparticles.

2.2. Synthesis of floating catalysts

The immobilization of Fe_2O_3 nanoparticles on Luffa sponges consists of two simple steps: precipitation and reflux heating process. In the first step, the pretreated Luffa sponges were impregnated in 200 mL of $Fe(NO_3)_3$ solution (0.5 mol·L^{-1}) for 1 hour. Afterwards, NaOH solution (1.5 mol·L^{-1}) was dropwise added to the above mixture up to pH 11 under regular stirring to produce a brown $Fe(OH)_3$ precipitate. In the next step, all the mixture was heated at reflux (~ 100 °C) for 2 hours to form Fe_2O_3 nanoparticles on the surface of Luffa fibers. The mixture was cooled to room temperature, then the Fe_2O_3-coated Luffa sponges were washed with deionized water until the pH of washing water reached 7. Finally, the sponges were dried at 150 °C for 1 hour and named as Fe_2O_3/Luffa-2. For the comparison, the uncoated Luffa sponges and the Fe_2O_3-coated Luffa sponges without reflux heating were also prepared and named as Luffa and Fe_2O_3/Luffa-0, respectively.

2.3. Material characterization

Powder X ray diffraction (XRD) was used to study the crystal structure and the phase composition of all Fe_2O_3/Luffa catalysts. These samples were dried in vacuum at 100 °C for 3 hours, ground to fine powder, and then analyzed by using a SIEMENS D5000 diffractometer (Bruker, Billerica, MA, USA) equipped with Cu Kα radiation (λ = 1.5406 Å). The applied current and the operating voltage were set at 40 mA and 45 kV, respectively. The morphology and the microstructure of our samples were observed by field emission scanning electron microscopy (FESEM) taken on a SU8000 microscope (Hitachi, Tokyo, Japan) at the accelerating voltage of 10 kV. The content of Fe species on the surface of Luffa fibers was determined by atomic absorption spectrometry (AAS) using an AA-6300 spectrometer (Shimadzu, Japan). Moreover, the Brunauer–Emmett–Teller surface area (S_{BET}) of Luffa sponges before and after depositing Fe_2O_3 nanoparticles were measured via nitrogen adsorption-desorption isotherms recorded on a Nova 1000e analyzer (Quantachrome, Boynton Beach, FL, USA) at 77 K.

2.4. Photo-Fenton catalytic tests

The photo-Fenton catalytic degradation of methyl orange (MO) over our floating Fe_2O_3/Luffa-X samples were carried out under both ultraviolet A light and visible light in the presence of oxalic acid as a radical-producing source. All the experiments were performed at room temperature controlled by a water circulation system. For each catalytic test, 8 pieces of Fe_2O_3/Luffa sponges were dispersed in a static glass reactor containing 250 mL aqueous solution of MO (10^{-5} mol·L^{-1}) and oxalic acid (10^{-3} mol·L^{-1}). The initial pH of this solution was adjusted at 6 using dilute solution of H_2SO_4 or NaOH. Before irradiation, the reaction solution was magnetically stirred in the dark for 1 hour to stabilize the adsorption of MO molecules on catalyst surface. Subsequently, an ultraviolet A (UVA) light lamp (9W Radium 78, 33.0 W·m^{-2}) or a visible light lamp (9W Osram Dulux S, 12.5 W·m^{-2}) was used to effectuate the photo-Fenton catalytic process. These lamps were set up at the height of 10 cm above the solution surface. During irradiation, 5 mL of dye solution was withdrawn from the reactor at certain intervals and its MO concentration was determined by Helios Omega UV–VIS spectrophotometer (Thermo Fisher Scientific, USA) at 464 nm (the maximum absorbance wavelength of methyl orange [16]).

3. Results and discussion

3.1. Characterization of floating catalysts

Fig. 1 shows the numerical photographs of Luffa sponges, Fe_2O_3/Luffa-0, and Fe_2O_3/Luffa-2 samples. It was observed that the uncoated sponges display a characteristic yellow color of dried Luffa fruits whereas Fe_2O_3/Luffa-0 sample presents a brown color, indicating the presence of Fe(III)-containing species on the Luffa fibers. Interestingly, when Fe_2O_3/Luffa sponges were heated at reflux for 2 hours, the brown color gradually turns into reddish brown. This color change suggests that there has been an evolution in crystal structure, morphology or quantity of Fe(III)-containing species on Luffa surface.

The morphology of Luffa and Fe_2O_3/Luffa sponges was examined by FESEM micrographs. As seen in Fig. 2a, the uncoated Luffa sponges possess a fibrous strand texture with high surface roughness. Such morphology is expected

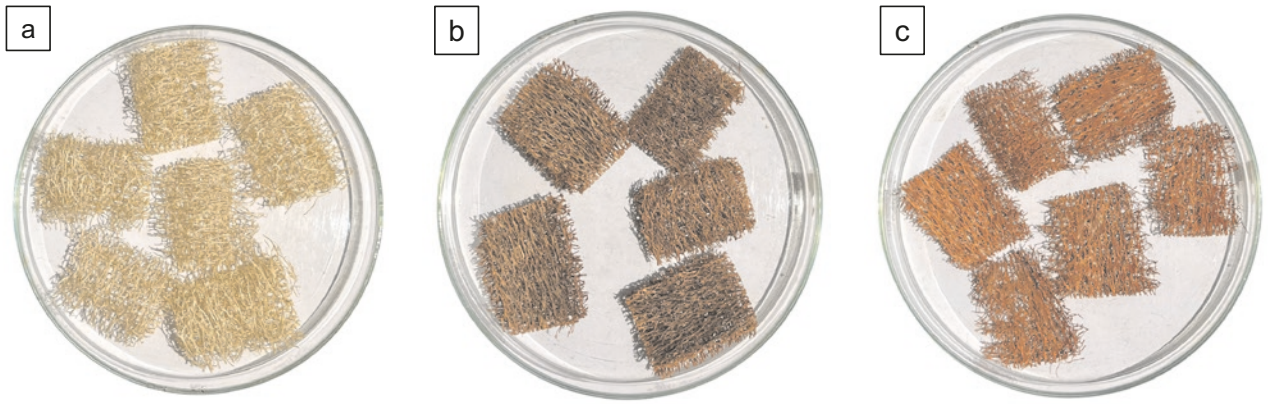

Fig. 1. Numerical photographs of Luffa (a), Fe_2O_3/Luffa-0 (b), and Fe_2O_3/Luffa-2 (c) sponges

to increase the surface accessibility towards Fe(III)-containing nanoparticles. In fact, the Fe_2O_3/Luffa-0 sample shows aggregates attached to the surface of Luffa fibers with the aggregate size of about 100 nm (Fig. 2b). These aggregates are composed of tiny particles joined together by sides, which are possibly assigned to Fe_2O_3 nanoparticles with low crystallinity degree. Moreover, in addition to the aggregates emerging on Luffa surface, a considerable quantity of nanoparticles seems to be mixed up underneath the Luffa fibers. Only when the Fe_2O_3/Luffa sponges were heated at reflux for 2 hours, the Fe_2O_3 nanoparticles were clearly seen with the polyhedral shape and the particle size ranging from 50 nm to 100 nm (Fig. 2c). These grown nanoparticles are still in agglomerated status but their grain boundaries can be easily observed, suggesting a good degree of crystallization for Fe_2O_3 nanoparticles in this sample.

The crystal structure and the phase composition of Luffa sponges and Fe_2O_3/Luffa samples were characterized through their XRD patterns (Fig. 3). The XRD pattern of Luffa sponges shows a characteristic behavior of cellulose I crystals with four diffraction peaks at 15.0°, 16.5°, 22.8°, and 34.5°, corresponding to (10), (110), (002), and (023) planes (space group *P-2*, JCPDS No. 03-0226). For Fe_2O_3/Luffa-0 sample, two additional weak peaks were observed at 33.1° and 35.6°, which can be attributed to the (104) and (110) planes of Fe_2O_3 hematite phase [17] (space group R-3c, JCPDS No. 86-0550). However, the intensity of these diffraction peaks is very low and the signal-to-noise ratio is also low, indicating the low crystallinity of Fe_2O_3 component. Conversely, the diffraction peaks of hematite phase and cellulose I phase in the XRD pattern of Fe_2O_3/Luffa-2 sample were clearly enhanced in intensity. This result confirms the fact that heating at reflux can be a simple method to improve the crystallinity of both Fe_2O_3 nanoparticles and cellulose fibers, which is in good agreement of FESEM study.

Since the changes in the morphology and the crystal structure of our catalytic samples can

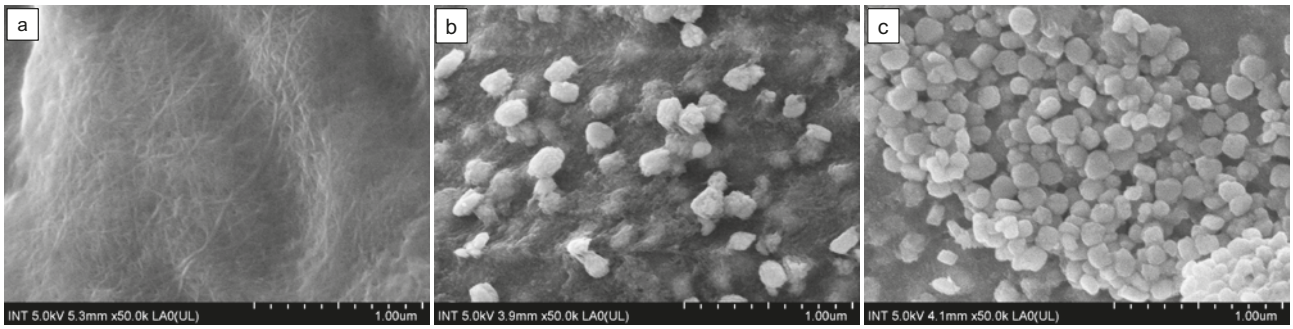

Fig. 2. FESEM micrographs of Luffa (a), Fe_2O_3/Luffa-0 (b), and Fe_2O_3/Luffa-2 (c) sponges

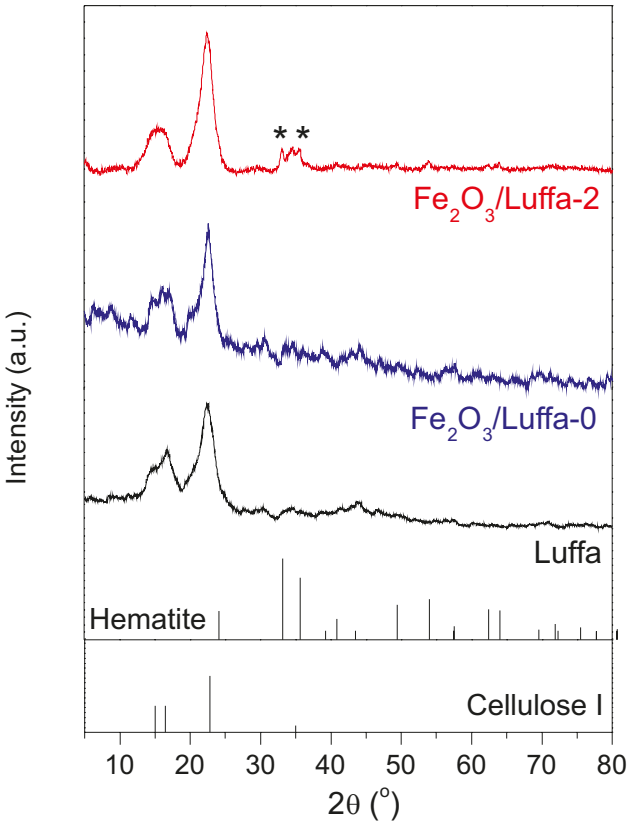

Fig. 3. XRD patterns of Luffa, Fe_2O_3/Luffa-0, and Fe_2O_3/Luffa-2 samples

affect their specific surface area, the nitrogen adsorption-desorption isotherm experiments were carried out. From these isotherms, the BET specific surface areas were calculated and shown in Table 1. Surprisingly, although the uncoated sponges show high surface roughness, their specific surface area is very restricted (0.554 $m^2 \cdot g^{-1}$). On the contrary, when Fe_2O_3 nanoparticles were immobilized on Luffa fibers, the specific surface was greatly enhanced. In fact, the Fe_2O_3/Luffa-0 sample displays the highest specific surface area (3.241 $m^2 \cdot g^{-1}$), which can be explained by the presence of numerous tiny particles on Luffa fibers. For Fe_2O_3/Luffa-2 sample, the specific surface area decreases, corresponding to the growth of Fe_2O_3 nanoparticles.

Table 1. Specific surface area and surface Fe content of Luffa, Fe_2O_3/Luffa-0, and Fe_2O_3/Luffa-2 samples

Sample	S_{BET} ($m^2 \cdot g^{-1}$)	Fe-content ($mg \cdot g^{-1}$)
Luffa	0.554	
Fe_2O_3/Luffa-0	3.241	58.2
Fe_2O_3/Luffa-2	1.820	36.3

Table 1 also reveals the Fe-contents, determined by AAS analysis, in Fe_2O_3/Luffa-0 and Fe_2O_3/Luffa-2 samples, proving the successful immobilization of Fe-containing species on the Luffa surface. Without heating at reflux, the content of Fe species on Luffa fibers (58.2 $mg \cdot g^{-1}$) is higher than that of Fe_2O_3/Luffa-2 sample (36.3 $mg \cdot g^{-1}$). This evolution supports the hypothesis that the reflux heating can help to grown Fe_2O_3 nanoparticles on Luffa fibers, but when the particles grow large enough, the van der Waals interactions between them and the fibers gradually weaken, making an amount of Fe_2O_3 particles possible to be removed from the fibers during the washing process.

3.2. Catalytic activity

Prior to illumination, the MO adsorption on the surface of our floating sponges was evaluated in the dark. At pH 6, all samples exhibited low MO adsorption percentages, and the difference in MO adsorption capacity between our samples is not significant (Table 2). Fig. 4a and 4b depicts time-dependent plots of MO degradation over our floating catalysts under UVA light and visible light, respectively. It was found that the MO concentration nearly remains unchanged during several hours of UVA-visible light exposure in the presence of oxalic acid and the uncoated Luffa sample, indicating that the direct self-photolysis of MO and the photo-Fenton catalytic activity of Luffa are negligible. Likewise, in the absence of oxalic acid, both Fe_2O_3/Luffa-0 and Fe_2O_3/Luffa-2 samples did not exhibit any activity for MO degradation under UVA light or under visible light. Only when using acid oxalic as a radical-producing source, these samples showed promising UVA-light-induced and visible-light-induced catalytic performance. The photo-Fenton degradation of MO was found to fit well with the pseudo-first-order kinetic model, which allows to evaluate the catalytic activity of our samples by their apparent rate constants (Table 2). Accordingly, the rate constants of MO degradation over Fe_2O_3/Luffa-2 catalyst were always higher than those over Fe_2O_3/Luffa-0 catalyst under both UVA and visible light illumination, pointing out that the reflux heating is an important factor for the improvement of our floating photo-Fenton catalysts.

Table 2. Comparison of MO adsorption percentage and rate constants of MO degradation over floating catalysts under visible light and UVA light in the presence of oxalic acid

	Sample				
	Luffa	Fe_2O_3/Luffa-0	Fe_2O_3/Luffa-2		
	pH 6	pH 6	pH 4	pH 6	pH 8
MO adsorption percentage (%)	9.5	11.6	14.5	10.8	3.9
Rate constant of MO degradation k (h^{-1}) under UVA light	No activity	1.174	0.591	1.461	No activity
Rate constant of MO degradation k (h^{-1}) under visible light	No activity	0.031	0.041		

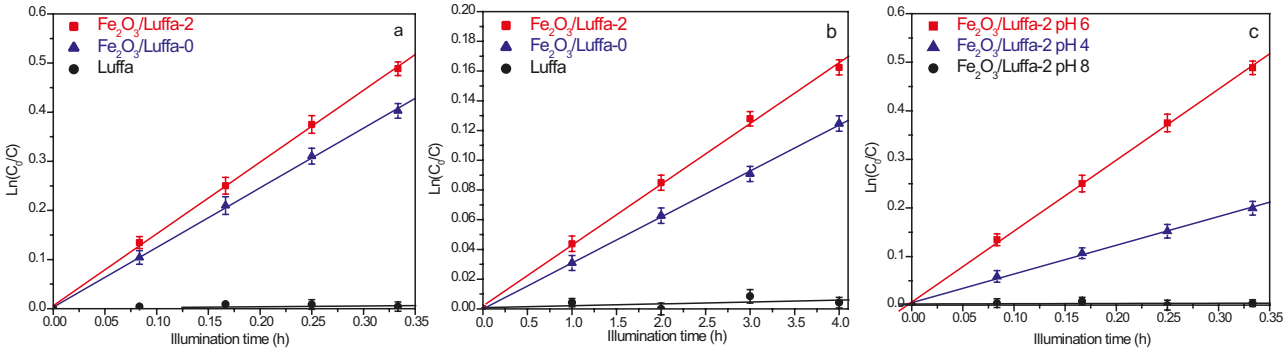

Fig. 4. Ln (C_0/C) versus time plot of oxalate-induced-MO degradation on floating catalysts under UVA light at pH 6 (a); under visible light at pH 6 (b); and under UVA light at different pH values (c). C is the MO concentration (mol·L^{-1}) at time t and C_0 is the initial MO concentration (mol·L^{-1}).

The influences of initial solution pH values on the MO adsorption and the photo-Fenton catalytic discoloration of MO over Fe_2O_3/Luffa-2 catalyst with oxalic acid were also investigated (Fig. 4c and Table 2). Accordingly, the MO adsorption on this catalyst tended to decrease with increasing pH of solution. In contrast, under UVA light illumination, the rate constant of MO degradation significantly increased from pH 4 (k = 0.591 h^{-1}) to pH 6 (k = 1.461 h^{-1}). However, at pH 8, no MO degradation was observed. These results indicate that our floating photo-Fenton catalysts can effectively operate at near neutral pH, but their performance is reduced at lower pH values or suppressed at basic medium.

3.3. Discussion

As shown in the experimental results of catalytic tests, the photo-Fenton catalytic degradation of MO only effectively occurs over floating Luffa sponges when these sponges were coated with Fe_2O_3 nanoparticles and exposed to light illumination in the presence of oxalic acid. This is most likely explained by the ability of surface Fe(III)-species to form ferrioxalate complexes with oxalate ions, which can be excited by light to initiate a series of reactions as follows [18]:

$$[Fe^{III}(C_2O_4)_2]^- + h\nu \rightarrow [Fe^{II}(C_2O_4)] + C_2O_4^{\bullet -}$$
$$k = 0.04\ s^{-1}\ [19] \quad (1)$$

$$C_2O_4^{\bullet -} + O_2 \rightarrow O_2^{\bullet -} + 2CO_2$$
$$k = 2.4{\cdot}10^9\ M^{-1}{\cdot}s^{-1}\ [20] \quad (2)$$

$$O_2^{\bullet -} + H^+ \rightarrow HO_2^{\bullet}$$
$$k = 6.3{\cdot}10^4\ M^{-1}\ [21] \quad (3)$$

$$HO_2^{\bullet} + HO_2^{\bullet} \rightarrow H_2O_2 + O_2$$
$$k = 8.3 \times 10^5\ M^{-1}\ [22] \quad (4)$$

$$[Fe^{II}(C_2O_4)] + H_2O_2 \rightarrow [Fe^{III}(C_2O_4)]^+ + OH^- + OH^{\bullet}$$
$$k = 3.1{\cdot}10^4\ M^{-1}{\cdot}s^{-1}\ [20] \quad (5)$$

Due to their high oxidizing capacity [23], the generated hydroxyl radicals are able to stimulate a fruitful degradation process for MO molecules. In fact, in order to justify the ability of our catalytic sponges to generate hydroxyl radicals, the scavenger tests were carried out by using tert-butyl alcohol as an agent to scavenge hydroxyl

radicals [24]. As shown in Table 3, when the molar concentration of tert-butyl alcohol gradually increased, the rate constant of MO degradation over Fe_2O_3/Luffa-2 catalyst was greatly reduced, proving that hydroxyl radicals play a vital role in the photo-Fenton catalytic performance of our floating catalysts.

Base on the above mechanism and the results of scavenger tests, the surface Fe(III)-species can be considered as the active centers for photo-Fenton processes in the presence of oxalic acid. It is also expected that the more the Fe_2O_3 nanoparticles are immobilized on the surface of Luffa fibers, the more the possibility of ferrioxalate complexation increases, which enhances the photo-Fenton catalytic activity. However, in this work, our Fe_2O_3/Luffa-2 catalyst always showed better performances than Fe_2O_3/Luffa-0 catalyst under both UVA light and visible light despite the fact that the Fe-content on the surface of Fe_2O_3/Luffa-2, determined by AAS technique, is inferior to that of Fe_2O_3/Luffa-0. Even, the floating catalyst prepared with reflux heating also showed a lower specific surface area than Fe_2O_3/Luffa-0 sample. These results indicate that there must be other factors besides Fe-content and specific surface area affecting the catalytic performances of our floating samples.

According to XRD and FESEM studies, the reflux heating used in the catalyst synthesis can improve the crystallinity of Fe_2O_3 nanoparticles on Luffa fibers, thereby reducing the bulk defects in the hematite lattice. This factor may be the main reason for the enhancement of photo-Fenton catalytic performance of Fe_2O_3/Luffa-2 sample. In the literature, although Fe_2O_3 was considered as a potential photocatalyst with a narrow bandgap (~2.2 eV), its photocatalytic activity was usually reported to be very low for practical applications due to its high electron-hole recombination and poor conductivity [25, 26]. Our work also proved that MO was not degraded by the photocatalytic activity of Fe_2O_3/Luffa sponges without oxalic acid as a radical-producing source. Nevertheless, we believe that the photocatalytic features of α-Fe_2O_3 nanoparticles still contribute to their photo-Fenton catalytic performances. It was noticed that the transformation from $[Fe^{III}(C_2O_4)_2]^-$ to $[Fe^{II}(C_2O_4)]$ (Eq. 1) is the slowest step in the oxalate-induced photo-Fenton catalysis whereas the consumption of $[Fe^{II}(C_2O_4)]$ (Eq. 5) is fairly fast, which potentially unbalances the whole process and then reduces the photo-Fenton activity. Fortunately, owing to the photocatalytic activity, Fe_2O_3 nanoparticles can be excited under light illumination to produce electron-hole pairs. For Fe_2O_3/Luffa-2 sample, since the Fe_2O_3 nanoparticles were well grown with high degree of crystallization, these photogenerated electrons are easily transferred to the oxide surface and react with $[Fe^{III}(C_2O_4)_2]^-$ to promote the regeneration of Fe(II)-species, which significantly enhances the catalytic performances. In contrast, without reflux heating, the Fe_2O_3 particles in Fe_2O_3/Luffa-0 sample are not grown enough to have a stable structure for the transfer of photogenerated electrons.

Furthermore, pH of reaction solution is also another important factor that needs to be taken into consideration for our photo-Fenton catalytic system. When the pH increases, the charge of our catalyst surface became less positive, more negative, which prevents the adsorption of anionic dyes such as MO molecules. As a result, the probability of hydroxyl radicals approaching MO molecules could be reduced. Moreover, based on the above-mentioned mechanism, especially on the Eq. 5, it is expected that the presence of OH^- ions at basic pH values will hinder the generation of hydroxyl radicals. This explains why our floating catalysts are almost inactive at pH 8. Interestingly, the experimental results indicated that the Fe_2O_3/Luffa-2 catalyst work best at near neutral pH (pH 6) instead of more acidic pH values (pH 4) although the MO adsorption capacity of the catalyst at pH 6 is lower than that at pH 4. This can be attributed to the weak acidity of oxalic acid. At acidic media, oxalic acid difficultly dissociates to

Table 3. Comparison of rate constants of MO degradation over Fe_2O_3/Luffa-2 catalyst under UVA light with tert-butyl alcohol at different molar concentrations

Scavenger tests				
[tert-butyl alcohol] ($mol \cdot L^{-1}$)	0	$5 \cdot 10^{-4}$	10^{-3}	$1.5 \cdot 10^{-3}$
Rate constant of MO degradation k (h^{-1})	1.461	0.574	0.442	0.350

form oxalate ions, which inhibits the formation of ferrioxalate complexes on the surface of our floating catalysts. Consequently, their photo-Fenton catalytic performance was declined.

3.4. Reuse tests

The reusability of our Fe_2O_3/Luffa-2 catalyst was evaluated through three repeated cycles. Since these sponges float on water surface (Fig. 5a), after each cycle, they were easily separated from the solution, washed with distilled water and reused directly for the next run. As shown in Fig. 5b, the rate constant of MO degradation considerably decreases from 1.461 to 0.890 h^{-1} at the second run and slightly decreases to 0.804 h^{-1} at the third run. This decline of photo-Fenton catalytic activity may be explained by the partial passivation of the catalyst surface due to the absorption of decomposition products. Nevertheless, our floating catalysts still exhibits promising performances for MO degradation after two-time reuses as well as facile recoverability, which minimizes negative impacts of Fe_2O_3 nanoparticles on the environment.

4. Conclusions

In this work, by using the simple precipitation-reflux heating method, we successfully prepared floating Fe_2O_3/Luffa sponges as effective oxalate-induced-photo-Fenton catalysts for the degradation of methyl orange under both UVA light and visible light. The reflux heating process in synthesis procedure was proved to increase the crystallinity of Fe_2O_3 nanoparticles on Luffa fibers, resulting in the enhanced catalytic performance. These catalysts sponges were also found to work best at near neutral pH, making them well suited for practical wastewater treatments. Moreover, since the catalytic sponges float on water surface, they are easily separated from the effluent and potentially reused for the next runs.

Contribution of the authors

The authors contributed equally to this article.

Conflict of interests

The authors declare that they have no known competing financial interests or personal relationships that could have influenced the work reported in this paper.

References

1. Shah M. Effective treatment systems for azo dye degradation: a joint venture between physico-chemical & microbiological process. *Journal of Environmental Bioremediation & Biodegradation*. 2014;2: 231–242. https://doi.org/10.12691/ijebb-2-5-4

2. Fan J., Guo Y., Wang J., Fan M. Rapid decolorization of azo dye methyl orange in aqueous solution by nanoscale zerovalent iron particles. *Journal of Hazardous Materials*. 2009;166: 904–910. https://doi.org/10.1016/j.jhazmat.2008.11.091

3. Haque M. M., Haque M. A., Mosharaf M. K., Marcus P. K. Decolorization, degradation and detoxification of carcinogenic sulfonated azo dye methyl orange by newly developed biofilm consortia. *Saudi*

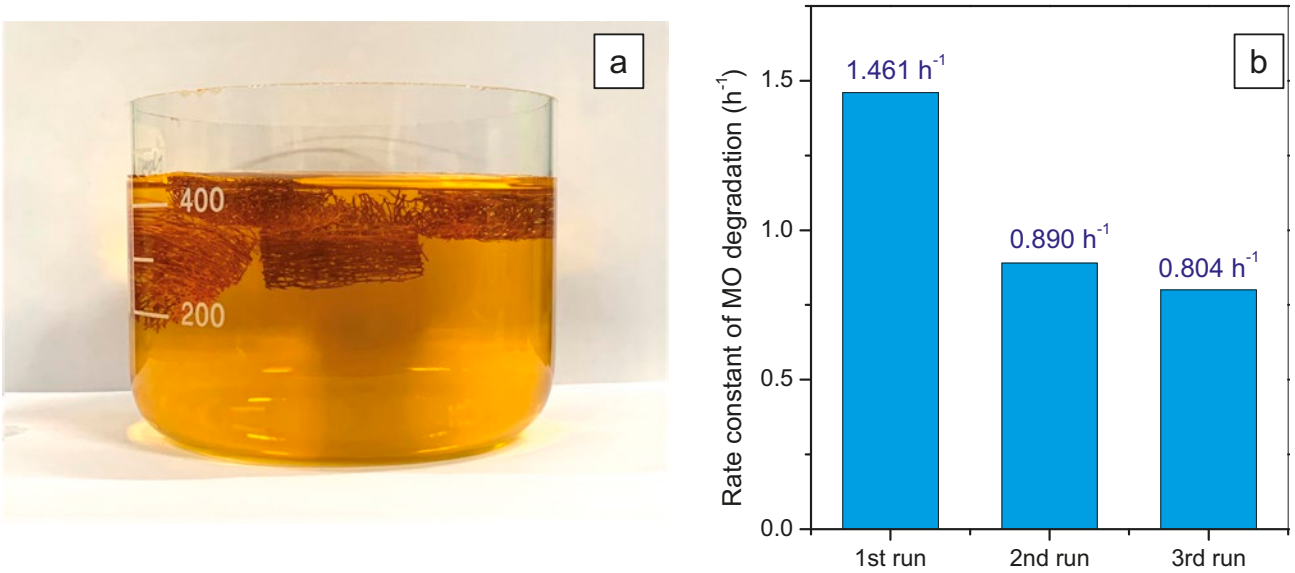

Fig. 5. Numerical photograph of Fe_2O_3/Luffa sponges floating on the surface of MO solution (a) and degradation of MO on Fe_2O_3/Luffa-2 catalyst in three consecutive experiments (b)

Journal of Biological Sciences. 2021;28: 793–804. http://doi.org/10.1016/j.sjbs.2020.11.012

4. Kant R. Textile dyeing industry an environmental hazard. *Natural Sciences*. 2012;4: 22–26. http://doi.org/10.4236/ns.2012.41004

5. Akansha K., Chakraborty D., Sachan S. G. Decolorization and degradation of methyl orange by Bacillus stratosphericus SCA1007. *Biocatalysis and Agricultural Biotechnology*. 2019;18: 101044. https://doi.org/10.1016/j.bcab.2019.101044

6. Stepanova K. V., Yakovleva N. M., Kokatev A. N., Pettersson, H. The structure and properties of nanoporous anodic oxide films on titanium aluminide. *Condensed Matter and Interphases*. 2019;21(1): 135–145. https://doi.org/10.17308/kcmf.2019.21/724

7. Xu Z. Zhang M., Wu J., Liang J., Zhou L., Lǔ B. Visible light-degradation of azo dye methyl orange using TiO2/β-FeOOH as a heterogeneous photo-Fenton-like catalyst. *Water Science & Technology*. 2013;68(10): 2178–2185. https://doi.org/10.2166/wst.2013.475

8. Hassan M. E., Chen Y., Liu G., Zhu D., Cai J. Heterogeneous photo-Fenton degradation of methyl orange by Fe_2O_3/TiO_2 nanoparticles under visible light. *Journal of Water Process Engineering*. 2016;12: 52–57. https://doi.org/10.1016/j.jwpe.2016.05.014

9. Domacena A. M. G., Aquino C. L. E., Balela M. D. L. Photo-Fenton degradation of methyl orange using hematite (α-Fe_2O_3) of various morphologies. *Materials Today: Proceedings*. 2020;22: 248–254. https://doi.org/10.1016/j.matpr.2019.08.095

10. Shaabani A., Nosrati H., Seyyedhamzeh M. Cellulose@Fe_2O_3 nanoparticle composites: magnetically recyclable nanocatalyst for the synthesis of 3-aminoimidazo[1,2-a]pyridines. *Research on Chemical Intermediates*. 2013;41: 3719–3727. https://doi.org/10.1007/s11164-013-1484-6

11. Mikenin P., Zazhigalov S., Elyshev A., Lopatin S., Larina T., Cherepanova S., Pisarev D., Baranov D., Zagoruiko A. Iron oxide catalyst at the modified glass fiber support for selective oxidation of H_2S. *Catalysis Communications*. 2016;87: 36–40. https://doi.org/10.1016/j.catcom.2016.08.038

12. Bian L., Liu Y., Zhu G., Yan C., Zhang J., Yuan A. Ag@$CoFe_2O_4$/Fe_2O_3 nanorod arrays on carbon fiber cloth as SERS substrate and photo-Fenton catalyst for detection and degradation of R6G. *Ceramics International*. 2018;44(7): 7580–7587. https://doi.org/10.1016/j.ceramint.2018.01.172

13. Mohamad E. R., Haidar Z., Lakiss L., Toufaily J., Frederic T. S. Immobilization of TiO_2 nanoparticles on natural Luffa cylindrica fibers for photocatalytic applications. *RSC Advances*. 2013;3: 3438–3445. https://doi.org/10.1039/C2RA22438K

14. Feng L., Zhang P., Li J., Han X., Tang S. Facile preparation, characterization, and formaldehyde elimination performance of MnO_x/natural loofah composites. *Environmental Progress and Sustainable Energy*. 2020;39(6): e13437. https://doi.org/10.1002/ep.13437

15. Annunciado T. R., Sydenstricker T. H. D., Amico S. C. Experimental investigation of various vegetable fibers as sorbent materials for oil spills. *Marine Pollution Bulletin*. 2005;50: 1340–1346. https://doi.org/10.1016/j.marpolbul.2005.04.043

16. Wu M. C., Lin M. P., Chen S. W., Lee P. H., Lic J. H., Su W. F. Surface-enhanced Raman scattering substrate based on a Ag coated monolayer array of SiO_2 spheres for organic dye detection. *RSC Advances*. 2014;4: 10043. https://doi.org/ 10.1039/c3ra45255g

17. Mittova I. Y., Sladkopevtsev B. V., Mittova V. O., Nguyen A. T., Kopeychenko E. I., Khoroshikh N. V., Varnachkina I. A. Formation of nanoscale films of the (Y_2O_3–Fe_2O_3) on the monocrystal InP. *Condensed Matter and Interphases*. 2019;21(3): 406–418. https://doi.org/10.17308/kcmf.2019.21/1156

18. Huang Y. H., Huang Y. J., Tsai H. C., Chen H. T. Degradation of phenol using low concentration of ferric ions by the photo-Fenton process. *Journal of the Taiwan Institute of Chemical Engineers*. 2010;41: 699–704. https://doi.org/10.1016/j.jtice.2010.01.012

19. Duesterberg C. K., Cooper W. J., Waite T. D. Fenton-mediated oxidation in the presence and absence of oxygen. *Environmental Science & Technology*. 2005;39: 5052–5058. https://doi.org/10.1021/es048378a

20. Mulazzani Q. G., D'Angelantonio M., Venturi M., Hoffman M. Z., Rodgers M. A. J. Interaction of formate and oxalate ions with radiation-generated radicals in aqueous solution. Methylviologen as a mechanistic probe. *Journal of Physical Chemistry*. 1986;90: 5347–5352. https://doi.org/10.1021/j100412a090

21. Walling C. Fenton's reagent revisited. *Accounts of Chemical Research*. 1975;8: 125–131. https://doi.org/10.1021/ar50088a003

22. Sedlak D. L., Hoigné J. The role of copper and oxalate in the redox cycling of iron in atmospheric waters. *Atmospheric Environment*. 1993;27: 2173–2185. https://doi.org/10.1016/0960-1686(93)90047-3

23. Wang X., Zhang L. Kinetic study of hydroxyl radical formation in a continuous hydroxyl generation system. *RSC Advances*. 2018;8: 40632. https://doi.org/10.1039/C8RA08511K

24. Biswas A., Saha S., Jana N. R. $ZnSnO_3$ nanoparticle-based piezocatalysts for ultrasound-assisted degradation of organic pollutants. *ACS Applied Nano Materials*. 2019;2: 1120–1128. https://doi.org/10.1021/acsanm.9b00107

25. Kormann C., Bahnemann D. W., Hoffmann M. R. Environmental photochemisty: Is iron oxide (hematite) an active photocatalyst? A comparative study: α-Fe_2O_3, ZnO, TiO_2. *Journal of Photochemistry and Photobio-*

logy A: Chemistry. 1989;48: 161–169. https://doi.org/10.1016/1010-6030(89)87099-6

26. Mishra M., Chun D. M. α-Fe_2O_3 as a photocatalytic material: A review. *Applied Catalysis A: General*. 2015;498: 126–141. https://doi.org/10.1016/j.apcata.2015.03.023

Information about the authors

Quynh Nhu Le Thi, 4th year student, Faculty of Chemistry, University of Science, Vietnam National University (Ho Chi Minh City, Vietnam).

ltqnhu2608@gmail.com

Thi Quynh Trang Ly, 3rd year student, Faculty of Chemistry, University of Science, Vietnam National University (Ho Chi Minh City, Vietnam).

lythiquynhtrang02@gmail.com

Anh Tien Nguyen, PhD in Chemistry, Chief of Inorganic Chemistry Department, Ho Chi Minh City University of Education Vietnam (Ho Chi Minh City, Vietnam).

tienna@hcmue.edu.vn

Quoc Thiet Nguyen, PhD in Chemistry, Institute of Applied Materials Science, Vietnam Academy of Science and Technology (Ho Chi Minh City, Vietnam).

ngqthiet@yahoo.com

De-Hao Tsai, PhD in Chemistry, Professor of Department of Chemical Engineering, National Tsing Hua University (Hsinchu, Taiwan, ROC).

dhtsai@mx.nthu.edu.tw

Tien Khoa Le, PhD in Chemistry, Chief of Inorganic Chemistry Department, University of Science, Vietnam National University (Ho Chi Minh City, Vietnam).

ltkhoa@hcmus.edu.vn

Received 16.05.2023; approved after reviewing 29.05.2023; accepted for publication 15.06.2023; published online 25.03.2024.